

Molecular Dynamics of the Diels–Alder Reactions of Tetrazines with Alkenes and N₂ Extrusions from Adducts

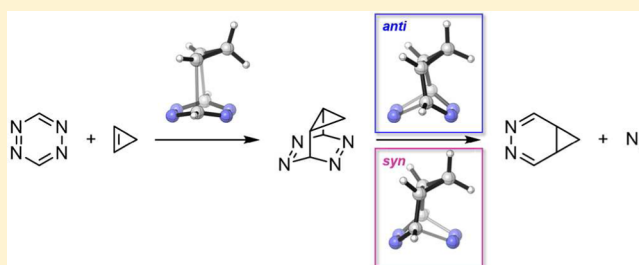
Lisa Törk,[†] Gonzalo Jiménez-Osés,[†] Charles Doubleday,[‡] Fang Liu,[†] and K. N. Houk^{*,†}

[†]Department of Chemistry and Biochemistry, University of California, Los Angeles, California 90095, United States

[‡]Department of Chemistry, Columbia University, New York, New York 10027, United States

S Supporting Information

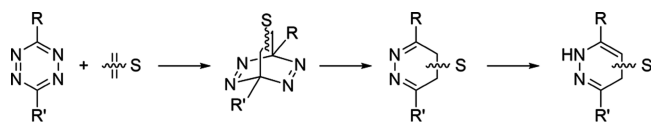
ABSTRACT: The cycloadditions of tetrazines with cyclopropenes and other strained alkenes have become among the most valuable bioorthogonal reactions. These reactions lead to bicyclic Diels–Alder adducts that spontaneously lose N₂. We report quantum mechanical (QM) and quasiclassical trajectory simulations on a number of these reactions, with special attention to stereoelectronic and dynamic effects on spontaneous N₂ loss from these adducts. QM calculations show that the barrier to N₂ loss is low, and molecular dynamics calculations show that the intermediate is frequently bypassed dynamically. There is a large preference for N₂ loss *anti* to the cyclopropane moiety rather than *syn* from adducts formed from reactions with cyclopropenes. This is explained by the interactions of the Walsh orbitals of the cyclopropane group with the breaking C–N bonds in N₂ loss. Dynamical effects opposing the QM preferences have also been discovered involving the coupling of vibrations associated with the formation of the new C–C bonds in the cycloaddition step, and those of the breaking C–N bonds during subsequent N₂ loss. This dynamic matching leads to pronounced nonstatistical effects on the lifetimes of Diels–Alder intermediates. An unusual oscillatory behavior of the intermediate decay rate has been identified and attributed to specific vibrational coupling.



INTRODUCTION

Since the initial report of inverse-electron-demand Diels–Alder reactions of tetrazines by Carboni and Lindsey in 1959,¹ extensive investigations of Diels–Alder reactions of tetrazines with a wide range of dienophiles have been reported, including applications in total synthesis.^{2–9} Sauer reported systematic kinetic studies of tetrazine cycloadditions to many types of alkenes and alkynes (Scheme 1) and large rate constants of Diels–Alder reactions between tetrazines and strained cyclic alkenes such as cyclopropene and *trans*-cyclooctene.³

Scheme 1. Reactions of Tetrazines with Alkenes



Two decades later, these extremely rapid cycloaddition reactions have been applied to bioorthogonal chemistry. Fox and Hilderbrand reported the success of tetrazine cycloadditions in live cell imaging, using *trans*-cyclooctene and norbornene as dienophiles.^{10,11} Since then, other strained alkenes and alkynes have been proposed and tested in the context of bioorthogonal reactions.^{12–14} Among them, cyclopropene derivatives are receiving much attention because of

their small sizes and low hydrophobicities, properties that lead to easy manipulation and good bioorthogonality.¹⁵

Our group explored theoretically the reactivities of tetrazines with strained alkenes in Diels–Alder reactions, and our interpretations and predictions have been confirmed by experimental observations.^{16–18} We have shown that the rapid rates of reactions of strained alkenes in Diels–Alder reactions with tetrazines originate in the ease of distortion of cyclopropenes into transition state (TS) geometries. Theoretical studies have focused on the Diels–Alder cycloaddition step, although subsequent N₂ loss and tautomerizations invariably occur in real systems.

Here we report quantum mechanics (QM) and quasiclassical trajectory (QCT) studies on the reactions between tetrazine and a series of alkenes, with cyclopropene being a key representative due to the importance of cyclopropenes in bioorthogonal chemistry.¹⁷ As a first step in understanding the dynamics of this process, the current QCT calculations are gas-phase simulations in the absence of explicit solvent molecules.

We first describe the QM potential energy surfaces (PESs) for the reactions between the parent tetrazine and cyclic and *cis*-alkenes. These and Birney's earlier¹⁹ calculations with alkynes reveal low barriers and high exothermicities for loss of N₂. Although loss of N₂ proceeds with a very low barrier, we

Received: January 7, 2015

Published: March 2, 2015

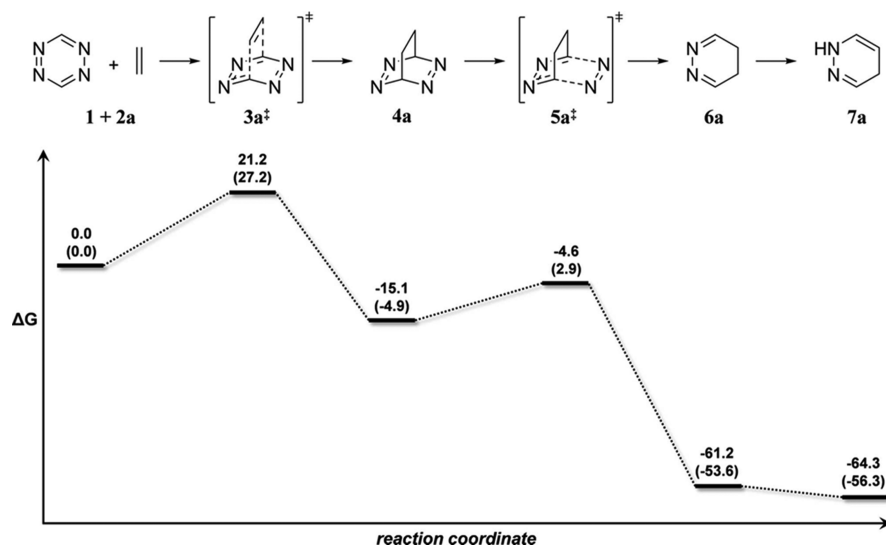


Figure 1. Energetics of the reaction of tetrazine and ethylene. Free energies (ΔG , in kcal mol^{-1}) at 298 K for each structure were calculated at the M06-2X/6-31G(d) and B3LYP/6-31G(d) (in parentheses) levels.

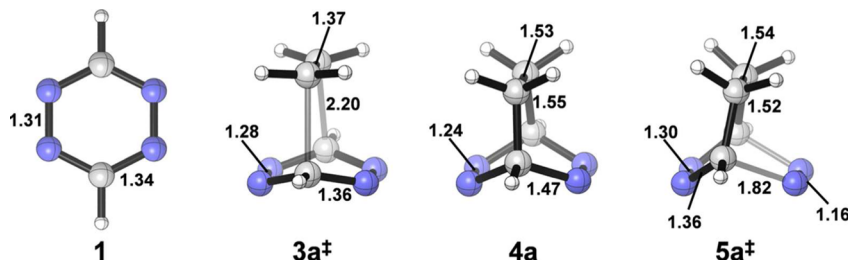


Figure 2. Geometries of tetrazine (1) and the transition structures and intermediate for the reaction with ethylene, calculated at the M06-2X/6-31G(d) level. Heavy-atom bond distances are shown in Å.

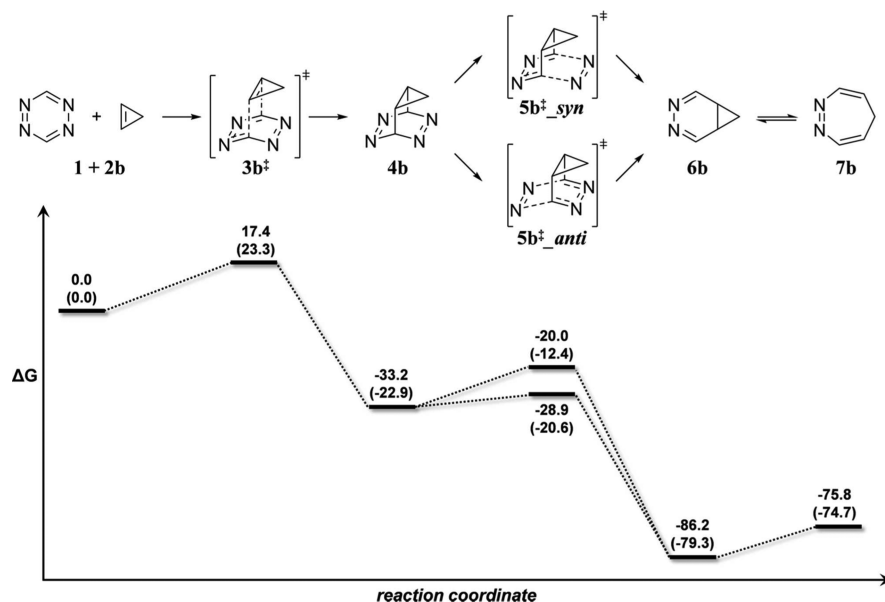


Figure 3. Energetics of the reaction of tetrazine and cyclopropene. Free energies (ΔG , in kcal mol^{-1}) at 298 K for each structure were calculated at the M06-2X/6-31G(d) and B3LYP/6-31G(d) (in parentheses) levels.

discovered a very large and unexpected regioselectivity in N_2 loss from cyclopropene Diels–Alder adducts. A detailed QCT study using density functional theory (DFT) forces for the reaction between parent tetrazine and cyclopropene was then carried out. These simulations uncovered significant non-

statistical dynamic effects on the lifetimes of the Diels–Alder intermediates and an unusual coupling of vibrational modes to decomposition rates. These studies are related to previous reports by Carpenter and others on the dynamics of N_2 extrusion to form diradicals,²⁰ although our systems are all

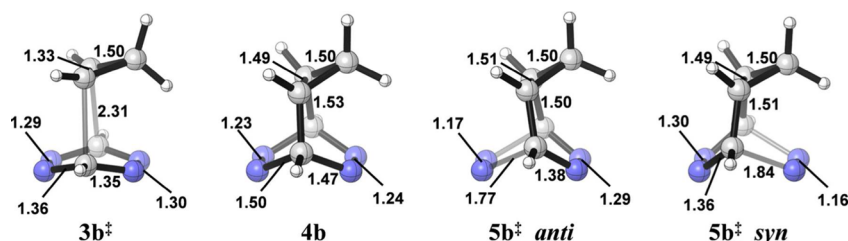


Figure 4. Geometries of transition structures $3b^\ddagger$, $5b^\ddagger_{syn}$, and $5b^\ddagger_{anti}$ and intermediate $4b$ calculated at the M06-2X/6-31G(d) level. Heavy-atom bond distances are shown in Å.

Table 1. Free Energies (ΔG , in kcal mol⁻¹) at 298 K Calculated with M06-2X/6-31G(d) for the Stationary Points in the Reactions of Tetrazine with Ethylene and Substituted Alkenes; B3LYP/6-31G(d) Results Are Shown in Parentheses

Stationary point					
3^\ddagger	21.2 (27.2)	17.4 (23.3)	21.4 (28.4)	25.6 (33.6)	23.9 (32.6)
4	-15.1 (-4.9)	-33.2 (-22.9)	-16.9 (-5.5)	-11.8 (1.2)	-9.8 (3.8)
5^\ddagger_{anti}	-4.6 (2.9)	-28.9 (-20.6)	-8.1 (0.4)	-2.9 (8.0)	1.9 (12.5)
5^\ddagger_{syn}		-20.0 (-12.4)	-3.8 (4.6)	-0.5 (10.7)	1.6 (12.5)
6	-61.2 (-53.6)	-86.2 (-79.3)	-61.5 (-53.6)	-56.9 (-46.7)	-56.7 (-46.2)

closed-shell throughout the whole reaction coordinate. Despite the very well-known dominant closed-shell character of these and related species, as a reviewer noted, the participation of radicals in this process cannot be conclusively ruled out in the absence of multi-reference calculations.

RESULTS

Potential Energy Surfaces for the Reactions of Tetrazines with Alkenes. The reaction between parent tetrazine and ethylene was studied first. Figure 1 shows the reaction pathway starting from parent tetrazine (**1**) and ethylene (**2a**), going through a TS, $3a^\ddagger$, to form bicyclic intermediate **4a**, and then through a *retro*-Diels–Alder TS, $5a^\ddagger$, to form product **6a**. This product can tautomerize into the more stable **7a**. These data indicate that the Diels–Alder cycloaddition is the rate-determining step, and that the barrier for the subsequent loss of N₂ is very small. Such a small barrier and large exergonicity of N₂ extrusion was also reported in a theoretical study of reactions between tetrazines and ethynylamine.¹⁹ The computed geometries of tetrazine (**1**), transition structures $3a^\ddagger$ and $5a^\ddagger$, and intermediate **4a** are shown in Figure 2.

We also explored the analogous reaction of tetrazine and cyclopropene and its energetics as shown in Figure 3. For reasons described earlier,^{16–18} cyclopropene reacts more readily than ethylene or less-strained *cis*-disubstituted alkenes to yield intermediate **4b**, which undergoes *retro*-Diels–Alder reaction through $5b^\ddagger$ to form **6b**.

This 3,4-diazanorcaradiene (**6b**) can undergo electrocyclic opening into **7b**, although with the parent tetrazine, this is an endergonic process.²¹ As observed with ethylene, the rate-determining step for the reaction between tetrazine and cyclopropene is the initial cycloaddition. The subsequent N₂ extrusion is predicted by these calculations to be highly selective depending on whether the leaving N₂ is *syn* or *anti* to the cyclopropane moiety in **4b**. The loss of N₂ located *anti* to the cyclopropane ring ($5b^\ddagger_{anti}$) is favored over the *syn* pathway ($5b^\ddagger_{syn}$), by about 9 kcal mol⁻¹ which would

correspond to a million times faster rate at room temperature. The products of both reaction pathways are, in this case, identical. The relevant structures calculated for these reactions are shown in Figure 4.

The reactions between tetrazine and cyclobutene, cyclopentene, and *cis*-butene were also studied. The free energies calculated for these reactions are summarized in Table 1. As noted previously by our group for related reactions,¹⁸ the cycloaddition step is highly influenced by the ease of alkene distortion. The activation barriers calculated here are highest for *cis*-butene (24 kcal mol⁻¹) and cyclopentene (26 kcal mol⁻¹), lower for cyclobutene (21 kcal mol⁻¹), and lowest for cyclopropene (17 kcal mol⁻¹). Ethylene is somewhat more reactive than the more sterically hindered and alkyl-stabilized *cis*-butene in spite of the greater electron-richness of the latter. More relevant to this work, the preference for *anti* loss of N₂ decreases as the size of cycloalkene reactant increases. The preference changes from $\Delta\Delta G_{anti/syn} = 9$ kcal mol⁻¹ for cyclopropene to 4, 3, and 0 kcal mol⁻¹ for cyclobutene, cyclopentene, and *cis*-2-butene, respectively.

The validity of the theoretical methods used in the QM calculations, and subsequently in the QCT studies, was confirmed by performing higher-level calculations with a long-range corrected functional including an empirical correction to dispersion (ω -B97x-D),²² and a correlated wave function method (SCS-MP2);²³ the larger basis set 6-311+G(2d,p) was used (see Supporting Information). B3LYP/6-31G(d), M06-2X/6-31G(d) and ω -B97x-D/6-311+G(2d,p) gave similar results in terms of the topology of the PES. As expected, with SCS-MP2/6-311+G(2d,p) the activation barriers were lower, but the complete *anti/syn* selectivity with cyclopropene was maintained ($\Delta\Delta G_{anti/syn}^\ddagger \approx 7$ kcal mol⁻¹).

Also, due to the poorly polar character of all the species involved in the calculated pathways (0–5 D), the influence of solvent polarity in the relative energies was calculated to be negligible even after geometry re-optimization in water using a continuum solvation method (PCM,²⁴ see Supporting In-

formation). In view of these results, the propagation of the QCTs in the gas phase at the computationally affordable B3LYP/6-31G(d) level, is justified.

Figure 5a shows a top view of $5b^{\ddagger}_{anti}$ and the σ^* and σ Walsh orbitals of the cyclopropane ring,²⁵ along with the σ and

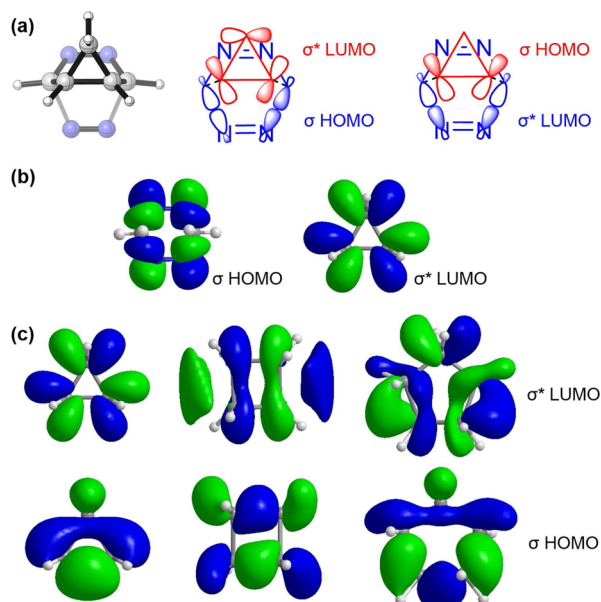


Figure 5. (a) Molecular orbital interactions responsible for the *anti* loss of N_2 . Left: LUMO of cyclopropyl fragment (red) and antisymmetric σ orbitals of breaking C–N bonds (blue). Right: HOMO of cyclopropyl fragment (red) and symmetric σ^* orbital of breaking C–N bonds (blue). (b) For comparison to the drawings in (a), the M06-2X HOMO of the 3,6-dihydro-tetrazine is shown to represent the tetrazine-derived fragment in **4b**, alongside the LUMO of cyclopropane to demonstrate the LUMO of the cyclopropene fragment in **4b**. (c) σ HOMOs and LUMOs of cyclopropane, cyclobutane, and cyclopentane calculated at the M06-2X/6-31G(d) level.

σ^* C–N orbitals of the breaking bonds *anti* to the three-membered ring in transition structure $5b^{\ddagger}_{anti}$. The blue and red orbitals in each diagram overlap very strongly in $5b^{\ddagger}_{anti}$, but overlap poorly in the corresponding $5b^{\ddagger}_{syn}$ (not shown here). These orbital interactions are responsible for the large preference for *anti* elimination of N_2 in the reaction of tetrazine and cyclopropene. The TS for the loss of N_2 located *syn* to the cyclopropane moiety ($5b^{\ddagger}_{syn}$) lacks such stabilizing orbital

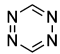
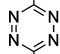
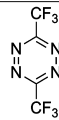
interactions due to poor orbital overlap. The *anti* C–N bond lengths in **4b** are somewhat larger than the *syn* bond lengths, another indication of this interaction between the Walsh orbitals and the *anti* C–N bonds even in the ground state of **4b**. Indeed, it is poised to break the *anti* C–N bonds!

Figure 5c shows the highest occupied and lowest unoccupied σ orbitals of cyclopropane, cyclobutane, and cyclopentane. As shown in Figure 5a, the cyclopropane Walsh orbitals overlap nearly perfectly with the breaking *anti* bonds but not the *syn*. As the ring size increases, the overlap between the relevant orbitals of cycloalkanes and the breaking *anti* σ^* C–N orbitals decreases, resulting in less facile N_2 extrusion. Also, the difference between *syn* and *anti* N_2 extrusion barriers disappears as this interaction becomes less important, and as the orbitals of the larger rings overlap equally well with both the *syn* and the *anti* C–N bonds.

We also studied the reactions between cyclopropene and substituted tetrazines—3,6-dimethyltetrazine (**8**) and 3,6-bis(trifluoromethyl)tetrazine (**9**)—to confirm that the phenomena we observed in the model system also apply to more realistic substituted systems used in experiments. Table 2 shows the cycloaddition/retro-cycloaddition activation energies. The observed substituent effects have been addressed in our previous study:¹⁸ electron-donating methyl substituents stabilize the tetrazine and raise cycloaddition reaction barriers, while electron-withdrawing trifluoromethyl groups have the opposite effects. The barriers for N_2 extrusion and the preference for the *anti* N_2 -extrusion pathway occur regardless of the substituent groups on the tetrazine.

Quasiclassical Trajectories for Cycloadditions and N_2 Extrusion. QCTs for the tetrazine–cyclopropene reaction were initialized at the saddle point $3b^{\ddagger}$ using TS normal-mode sampling,²⁶ as implemented in a customized version of the Venus dynamics package.²⁷ In QCT, the initial coordinates and momenta are chosen in a way that includes zero-point energy (ZPE) and thermal energies, in order to mimic a quantum Boltzmann distribution of vibrational levels. Trajectories were propagated with Gaussian 09,²⁸ which implements the Hessian-based predictor–corrector of Schlegel, Hase, and co-workers²⁹ invoked by the BOMD keyword. A total of 512 trajectories were propagated, each consisting of a forward and reverse segment. For a given set of initial coordinates and momenta, each trajectory was propagated until either reactants **1** and **2b** or product **6b** was formed; then the sign of the initially sampled momentum was reversed, and the trajectory propagated²⁷ from the initial geometry in reverse until either reactants **1** and **2b** or

Table 2. Free Energies (ΔG , in kcal mol⁻¹) at 298 K Calculated with M06-2X/6-31G(d) for the Stationary Points in Reactions of Cyclopropene with Tetrazine, 3,6-Dimethyltetrazine, and 3,6-Bis(trifluoromethyl)tetrazine; B3LYP/6-31G(d) Results Are Shown in Parentheses

Stationary point			
3^{\ddagger}	17.4 (23.3)	18.9 (26.8)	9.7 (17.5)
4	-33.2 (-22.9)	-30.0 (-17.4)	-45.0 (-31.5)
5^{\ddagger}_{anti}	-28.9 (-20.6)	-26.0 (-15.8)	-40.7 (-29.5)
5^{\ddagger}_{syn}	-20.0 (-12.4)	-18.4 (-8.9)	-31.8 (-21.5)
6	-86.2 (-79.3)	-84.5 (-76.8)	-96.8 (-89.1)

product **6b** was formed. A full trajectory was retained if the forward and reverse segments connected reactants **1** and **2b** with product **6b**. There were 450 such trajectories, while 62 involved recrossings or simply unproductive trajectories. The energy, gradient, and Hessian were calculated using the B3LYP functional and 6-31G(d) basis set.²⁸ These techniques have been applied by our group to other cycloadditions and molecular rearrangements.^{30–32}

The same methods were used for the single trajectory (ST) simulation; the ST is also initialized at the $3b^\ddagger$ saddle point and performed for the forward and backward directions. The ST is propagated with no vibrational, even ZPE, or rotational energy. Only 0.6 kcal mol⁻¹ energy is included in the reaction coordinate (the *RT* value at 298 K).

Rice–Ramsperger–Kassel–Marcus (RRKM) calculations were carried out for $4b \rightarrow 5b^\ddagger_{syn}$ and $4b \rightarrow 5b^\ddagger_{anti}$ using the Beyer–Swinehart direct count algorithm.^{33,34} The energy of **4b** was the ZPE-corrected energy difference of $3b^\ddagger$ and **4b**.

To apply Eyring's transition state theory (TST), activation free energies (ΔG^\ddagger) between intermediate **4b** and TS $5b^\ddagger$, were used to compute rate constants.

Quasiclassical dynamics performed at 25 °C show that, out of 450 productive trajectories started from $3b^\ddagger$, 92 (20%) passed through the high $5b^\ddagger_{syn}$ barrier after **4b** formation, while 358 (80%) traversed through the lower energy TSs $5b^\ddagger_{anti}$. This leads to a predicted *anti:syn* ratio of 4:1, very different from the 4,000,000:1 ratio predicted by TST for a 9 kcal/mol⁻¹ difference in ΔG^\ddagger at 298 K. Such nonstatistical dynamics are well known for chemically activated short-lived intermediates.^{35–37}

In order to assess the inherent dynamical preferences imposed by the PES on the *anti* and *syn* reaction channels, we propagated a ST without vibrational energy, not even ZPE, from $3b^\ddagger$ toward **4b**. Trends in vibrational, rotational, and translational energy partitioning derived from this ST method have been shown to track the mean energy partitioning derived from QCTs.^{38–40,32c,b} For this reason, an ST is useful for condensing the complexities of QCTs into the dynamically favored motions. Strikingly, the ST releases N₂ via the higher energy $5b^\ddagger_{syn}$ pathway, demonstrating a dynamical preference for this reaction channel. Figure 6 shows local stretching mode energies of the forming and breaking bonds during the ST (one of the C–C bonds formed at $3b^\ddagger$, one of the C–N *anti* bonds

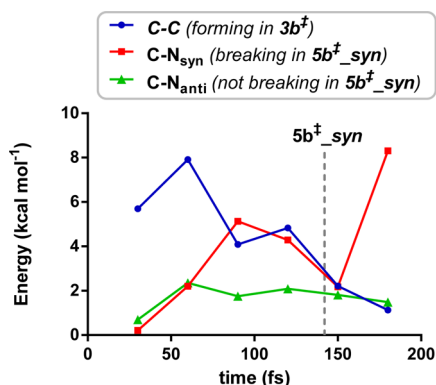


Figure 6. Evolution of local bond energies derived from a single trajectory (ST) involving only translational energy (*RT*) in the reaction coordinate. The dashed gray line depicts the time at which the ST passes through transition state $5b^\ddagger_{syn}$.

broken at $5b^\ddagger_{anti}$ and one of the C–N *syn* bonds broken at $5b^\ddagger_{syn}$).

After passage through $3b^\ddagger$, almost all of the energy is localized in the newly formed C–C bond. This energy arises from the translational motion of the two reactants toward each other, and this motion becomes a symmetric C–C stretch in the product. The energy then preferentially channels into the breaking *syn* C–N bond, which breaks readily due to this high vibrational excitation. This explains why there is a dynamical preference for the highly energetic $5b^\ddagger_{syn}$ pathway, but the $5b^\ddagger_{anti}$ channel is still preferred in the quasiclassical trajectories, although much less than expected from the QM energetics.

The vibrational normal modes sampled at $3b^\ddagger$ that lead to either *syn* or *anti* N₂ extrusion were analyzed. There is one specific mode at $3b^\ddagger$ (ν_3), that is correlated with the $5b^\ddagger_{syn}$ pathway; i.e., it is dominantly excited in the starting structures of the TS ensemble leading to $5b^\ddagger_{syn}$ trajectories. This normal mode can be described as a symmetric rocking of the cyclopropane with respect to the tetrazine that alters the distance between N *syn* and the H on cyclopropane apex. This motion leads to steric clashing between these two fragments, which is relieved by stretching the *syn* C–N bonds, inducing *syn* N₂ loss.

On the other hand, normal mode ν_6 , when excited, leads mostly to trajectories involving loss of the *anti* N₂. This vibration can be described as an asymmetric stretching of the two forming C–C bonds, since one forming C–C bond is shortened and the other is lengthened. This asymmetric stretch of the forming bonds enhances the interaction of the cyclopropane Walsh orbitals with the *anti* C–N bonds when intermediate **4b** is reached, and this enhances the preference predicted from the QM calculations. Both vibrational modes are shown in Figure 7. Notably, mode ν_3 is 1.6 times more

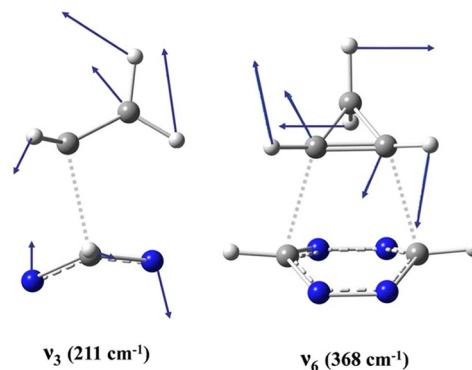


Figure 7. Vibrational modes in $3b^\ddagger$ that are frequently associated with *syn* and *anti* N₂ extrusion pathways. Mode ν_3 leads preferentially to $5b^\ddagger_{syn}$ and mode ν_6 to $5b^\ddagger_{anti}$. Mode ν_3 is viewed along an axis perpendicular to the symmetry plane (six atoms are eclipsed and not visible).

excited in the transition structures leading to *syn* than to *anti* trajectories, while mode ν_6 is 1.9 times more excited for *anti* than for *syn* trajectories.

Diels–Alder Intermediates Show Strong Nonstatistical Behavior. Transition zones were defined for the C–C forming (3^\ddagger) and the C–N breaking (5^\ddagger) steps (see Supporting Information for details). The TS zone for $3b^\ddagger$ is the region where the forming C–C bond lengths are within the 98th percentile of the normal-mode sampling distribution at the

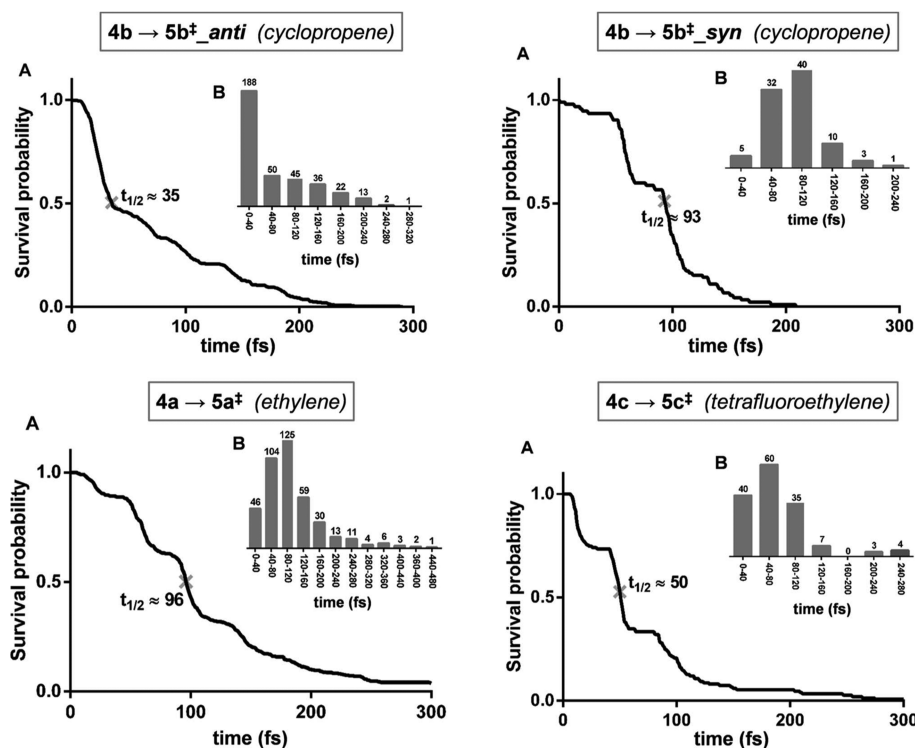


Figure 8. (A) Survival probability plots for the intermediates **4a–c** (fraction of trajectories that have formed **4a–c** but have not formed **6** vs time) generated in the cycloaddition reactions of tetrazine (**b**) (*anti* and *syn* refer to the stereochemistries of the N_2 extrusion pathways), ethylene (**a**), and tetrafluoroethylene (**c**) derived from the QCT. The half-life times for each respective reaction ($t_{1/2}$) are depicted. (B) The numbers of trajectories that expel N_2 in intervals of 40 fs are shown as insets on each plot.

saddle point of $3b^{\ddagger}$. Similarly, we define the transition zones for *syn* and *anti* $5b^{\ddagger}$ as the geometries within the 98th percentile of the normal-mode sampling distribution with respect to the breaking C–N bond at the saddle point of $5b^{\ddagger}$.³² The distance distributions are 2.30 ± 0.25 Å for $3b^{\ddagger}$, 1.76 ± 0.14 Å for $5b^{\ddagger}_{anti}$ and 1.85 ± 0.18 Å for $5b^{\ddagger}_{syn}$. The times to traverse the transition zones essential with $3b^{\ddagger}$ and $5b^{\ddagger}$ are 53 ± 1 and 107 ± 6 fs, respectively, for the *anti* processes, and 56 ± 1 and 63 ± 3 fs, respectively, for the *syn*. The lifetime of intermediate **4b** was defined as the elapsed time between departure from the transition zone $3b^{\ddagger}$ and entrance in transition zones $5b^{\ddagger}$. Figure 8 shows details about the decay of the intermediate **4b** lifetime through *anti* and *syn* N_2 eliminations. Considering the typical period of a single C–C bond stretching (~ 60 fs), 58% of the productive trajectories passing through $5b^{\ddagger}_{anti}$ can be regarded as dynamically concerted, a terminology that we have defined as multiple bonding changes occurring on a time scale faster than a C–C vibration.³¹ These trajectories skip intermediate **4b** completely. For the trajectories passing through the higher energy $5b^{\ddagger}_{syn}$, 70% are dynamically stepwise, and these sample the intermediate minimum.

In order to monitor the dynamical effect of a change of the mass of the alkene resulting from substitution, the related quantities for reactions of ethylene (**2a**) and tetrafluoroethylene (**2c**) are also compared in Figure 8 (see QM energies in Supporting Information).

We have also analyzed many of the typical representative trajectories for these reactions to give a more detailed picture of how these reactions occur. Figure 9 represents typically stepwise trajectories (in green) where the C–C bonds are formed first to yield intermediate **4b**; after spending about 200–300 fs vibrating in the intermediate region, it goes over

$5b^{\ddagger}_{anti}$ to form product **6b**. The same plot shows an example of concerted trajectories (in red) in which no intermediate vibrations occur after C–C bonds formation, and product **6b** is formed directly through $5b^{\ddagger}_{anti}$, as well as trajectories (blue) which are in between stepwise and fully concerted trajectories. The very small intermediate lifetimes derived from the QCTs, compared to those expected from TST or RRKM theory (Table 3, see discussion below), clearly reveal the existence of nonstatistical dynamic effects in this reaction. This behavior was also found in the reactions of tetrazine (**1**) with ethylene (**2a**) and tetrafluoroethylene (**2c**), whose dynamic profiles were studied in the same manner as those for cyclopropene (**2b**).

Table 3 shows lifetimes of Diels–Alder adduct **4** produced by tetrazine cycloadditions with the three alkenes (**2a–c**) computed with B3LYP/6-31G(d) at four levels of dynamical theory: canonical (298 K) and microcanonical quasiclassical trajectories (QCT and μ QCT) and canonical and microcanonical statistical theory (TST and RRKM). In TST, **4** is assumed to be at equilibrium with its surroundings at 298 K; the other methods do not incorporate that assumption. The QCT decays at 298 K are strongly nonexponential (Figure 8), and are not characterized by lifetimes. To summarize the dynamics in a single table entry, we used the formal definition of lifetime (time required to decay to $1/e$ of the starting population). μ QCTs were initialized with microcanonical quasiclassical TS normal-mode sampling⁴¹ at a total energy 2.3 kcal mol⁻¹ (the average vibrational excitation at 298 K) above the ZPE of $3b^{\ddagger}$. This energy matches the total energy used in RRKM calculations. Comparison of μ QCT and RRKM lifetimes shows a factor of 2 difference in lifetimes of **4b** with respect to passage over the small barrier $5b^{\ddagger}_{anti}$, but a factor of 10 difference for passage over the larger barrier $5b^{\ddagger}_{syn}$.

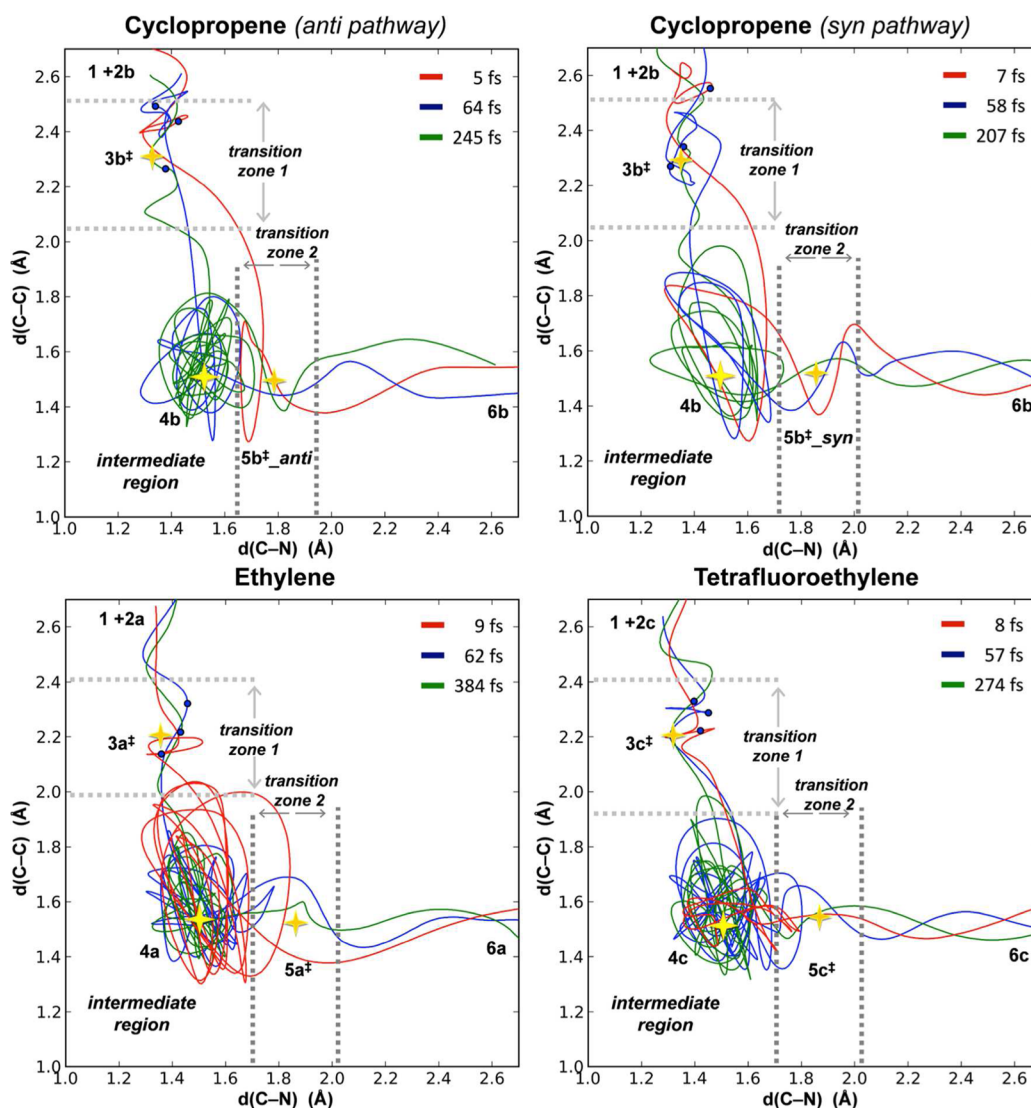


Figure 9. Representative trajectories for the dynamically concerted (red), stepwise (green), and borderline (blue) reaction pathways for tetrazine (1) + cyclopropene (2b), ethylene (2a), and tetrafluoroethylene (2c) cycloadditions. Yellow stars are the positions of the stationary points (transition structures or intermediates) and blue circles are the starting points of the trajectories shown.

Table 3. Lifetimes (fs) of Local Minimum 4 Computed at Four Levels of Dynamical Theory with B3LYP/6-31G(d)

	QCT ^a	μ QCT ^b	RRKM ^c	TST ^d
cyclopropene (<i>anti</i>) ^e	90 ± 10	160 ± 10	87	6794
cyclopropene (<i>syn</i>) ^f	100 ± 10	210 ± 10	2195	7.9 × 10 ⁹
tetrafluoroethylene	85 ± 10		558	1.6 × 10 ⁷
ethylene	120 ± 10		1400	1.6 × 10 ⁸

^aQCTs initialized at TS 3[‡] at 298 K. Lifetimes are nonexponential.

^bInitialized at 3b[‡] with microcanonical quasiclassical TS normal-mode sampling (ref 41) with total energy 2.3 kcal mol⁻¹ above ZPE. Lifetimes are nonexponential. ^cTotal energy is 2.3 kcal mol⁻¹ above the ZPE of 3[‡]. ^d4 is assumed to be at equilibrium with its surroundings at 298 K. ^eLifetime of 4b with respect to passage through 5b[‡]_{anti}.

^fLifetime of 4b with respect to passage through 5b[‡]_{syn}. The statistical error of the QCT and μ QCT lifetimes (±10 fs) was considered to be equal to the bin width used in calculating the survival probabilities.

This is consistent with a dynamical preference for passage over the higher barrier. Since the QCTs decay nonexponentially, their lifetimes in Table 3 do not reflect the relative yields of passage through 5b[‡]_{anti} and 5b[‡]_{syn}. Direct trajectory counts

give an *anti/syn* ratio of 4 ± 1 for QCTs at 298 K and 8 ± 3 for μ QCTs. The latter is substantially different from the *anti/syn* ratio of 25:1 from RRKM lifetimes at the same total energy as the μ QCTs, and demonstrates a clear dynamical preference for the higher *syn* barrier under these conditions.

During an enlightening discussion on the existence of dynamical effects affecting the regioselectivity of hydroboration reactions,^{42–44} Glowacki et al. proposed that vibrationally excited intermediates can enter diverging pathways at different rates while they are cooled by collision with solvent molecules, translating into a nonstatistical regioselectivity.⁴⁴ Although the present study only refers to reactions in the gas phase, we tested the possibility of solvent collisions affecting the *anti/syn* reactive flux ratio by solving the energy-grained Master Equation for a range of excess reactant concentrations and collision rates ($\sim 10^7$ to $\sim 10^{17}$ s⁻¹) with a He bath using the Mesmer software⁴⁵ (see Supporting Information). In all realistic cases, the *anti/syn* ratio of rates was calculated to be 96:4, identical to the zero-pressure RRKM ratio. Collisional effects on selectivity can be, thus, discarded for this reaction, at least from the RRKM theory perspective.

The combination of strongly nonexponential decay in Figure 8, large difference in μ QCT vs RRKM lifetimes in Table 3, the difference in *anti/syn* yield ratios for μ QCTs vs RRKM at identical total energies, and the differences in lifetimes for 298 K QCTs vs. RRKM in Table 3, describe a strongly nonstatistical set of Diels–Alder adducts 4.

The survival probabilities of the intermediates 4 (fraction of trajectories that have not formed product 6 vs time) show a quite unusual behavior (Figure 8). Instead of typical mono- or biexponential decays, step functions were obtained. Oscillatory decay gated by vibrational modes is well known experimentally⁴⁶ and has been reported in trajectory simulations of organic reactions.^{32b,47–49} Figure 10 shows the lifetime

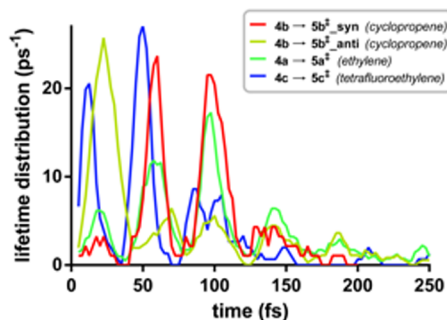


Figure 10. Lifetime distributions of the intermediates generated in the reactions between tetrazines and cyclopropene (4b), ethylene (4a), and tetrafluoroethylene (4c), derived from QCT. The zero in the X-axis was set to the time for passage over the cycloaddition barrier (3^{\ddagger}).

distributions of the intermediates for these reactions. The lifetime distribution $P(t) = -(1/N(0)) dN(t)/dt$ is the negative derivative of the survival probability $N(t)/N(0)$, where $N(t)$ is the number of trajectories that have not yet formed a product at time t . $P(t)$ oscillates as expected from the step character of the survival probabilities.

The oscillation period (~ 40 fs) is common for all systems. This observation implies that the same vibrational mode gates the decomposition of all of the intermediates, and thus their lifetimes. This gating mode was found to be the stretching vibration of the newly formed C–C bonds in intermediates 4. The relationship between the C–C bond length (that oscillates during vibration) and the decay of the intermediate is shown in Figure 11 for the reaction of tetrazine (1) and cyclopropene (2b) following the *anti* N_2 extrusion pathway.

The C_1 – C_2 bond length oscillates approximately in parallel with the lifetime distribution, first in an anticorrelated manner (intermediate disappears when the bond is compressed) and in a correlated manner after ~ 100 fs (intermediate disappears when the bond is elongated). This behavior is related to our previous observation that the C–C vibration, excited as the bimolecular collision energy is transformed into vibrational energy in the product, is transferred into energy of the C–N stretch that ultimately leads to N_2 loss.

CONCLUSION

We have explored the cycloadditions of tetrazine with representative dienophiles and subsequent loss of N_2 from the Diels–Alder adducts. Our focus has been on the reactions of cyclopropene, derivatives of which are now commonly used in bioorthogonal chemistry. The Diels–Alder reactions of tetrazine with dienophiles 2, such as cyclopropene, at 298 K

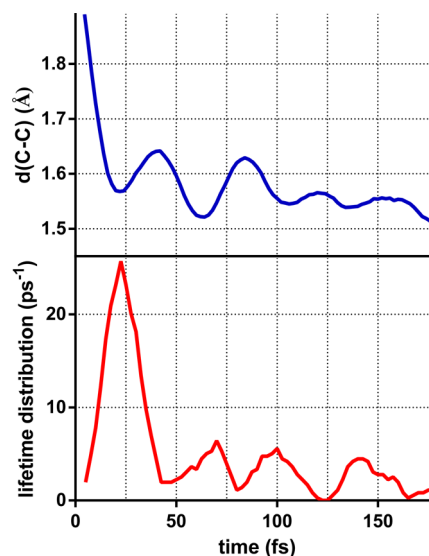


Figure 11. Intermediate 4b lifetime distribution and average C–C bond distance for the reaction between tetrazine and cyclopropene resulting in the *anti* extrusion pathway. The C–C bond distance was calculated by averaging the C–C distance at every step over all trajectories. The zero in the X-axis was set to the time for passage over the cycloaddition barrier (3^{\ddagger}).

lead to chemically activated bicyclic adducts 4 that exhibit strongly nonstatistical dynamics. For most reactions, the mechanism is actually a distribution of mechanisms, from dynamically concerted formation of 4 and release of N_2 to a clearly stepwise mechanism with a longer-lived adduct. We have discovered a stereoelectronic effect of the cyclopropene group in intermediate 4b, which strongly facilitates loss of *anti* N_2 from the intermediate adduct. Counteracting this stereoelectronic effect to some extent, there is a 10^6 -fold dynamical preference for the higher energy *syn* N_2 extrusion. This stresses the major role of dynamical effects in coupled cycloaddition/retro-cycloaddition reactions. Irrespective of the level of theory used in the quantum mechanical optimizations, dynamical effects should be taken into account to properly describe the behavior of very reactive intermediates, in which significant energy from previous steps is accumulated.

Finally, we have found that the intermediate adducts 4 decay in a stepwise fashion. That is, the lifetime distributions of the bicyclic adducts are oscillatory, with a periodicity that indicates that the decays are gated by the C–C stretching mode.

Although solvent polarity effects are negligible for these reactions involving very nonpolar transition states and intermediates ($\mu < 5$ D), the influence of collisional relaxation with the solvent remains an open question that is gaining increasing attention.^{50,51} Thus, the transferability of these gas-phase results to the condensed phase will be explored in the near future by means of hybrid QM/MM approaches as feasible methods become available.

EXPERIMENTAL SECTION

Quantum Mechanical Methods. All DFT calculations were performed with Gaussian 09.²⁸ Geometry optimizations of all the minima and TSs were carried out at the M06-2X⁵² level of theory with the 6-31G(d) basis set, which has been found to give relatively accurate energetics for cycloadditions.^{53,54} The vibrational frequencies were computed at the same level to verify that optimized structures are energy minima or TSs and to evaluate zero-point vibrational energies and thermal corrections at 298 K. A quasiharmonic correction was

applied during the entropy calculation by setting all positive frequencies that are less than 100 cm^{-1} to 100 cm^{-1} .⁵⁵ Results are also reported using the B3LYP⁵⁶ functional with the 6-31G(d) basis set. This functional and basis set were used for subsequent trajectory simulations, since it is substantially more economical than the more accurate M06-2X functional. Our previous studies showed that for Diels–Alder cycloaddition reactions, B3LYP overestimates the barriers by about 5 kcal mol^{-1} and underestimates the reaction exothermicity by about 10 kcal mol^{-1} .⁵⁷ Systematic errors found there are confirmed in this particular reaction between parent tetrazine and ethylene. The barrier for the cycloaddition step ($3a^\ddagger$) calculated with B3LYP is 6.0 kcal mol^{-1} higher than with M06-2X; the energy of cycloadduct **4a** computed with B3LYP is $10.2\text{ kcal mol}^{-1}$ higher than with M06-2X.

Method for Transition-State Normal-Mode Sampling at a Given Temperature. For each normal mode i , the number of vibrational quanta is sampled from a harmonic quantum Boltzmann distribution. The energy of mode i is randomly assigned to kinetic and potential energy, and the resulting normal-mode coordinates Q_i and momenta P_i are randomly assigned a phase. Cartesian coordinates q_i and momenta p_i are obtained by transforming Q_i and P_i by the eigenvectors of the harmonic force constant matrix. This transformation is not exact because vibrations are anharmonic, and energy E_{traj} obtained by the transformation usually differs from the energy E_{chosen} selected by sampling. The q_i and p_i are then scaled by a factor $(E_{\text{traj}}/E_{\text{chosen}})^{1/2}$, and the process is iterated a few times until E_{traj} is within 0.1% of E_{chosen} . The process is repeated for all $3N-7$ bound modes. For the transition vector, the kinetic energy is sampled from a classical Boltzmann distribution at temperature T .

Method for Computing Normal-Mode Energies during Trajectories. The procedure is based on the Raff velocity projection method.⁵⁸ In the present paper, the method is used to compute mode energies of trajectories that are initialized at 3^\ddagger and subsequently move within **4**, the Diels–Alder intermediate. Two files are needed: a trajectory file containing coordinates and momenta vs time, and a file with the optimized geometry and normal-mode eigenvectors of **4**. At each time t , the Cartesian velocities are projected onto each normal-mode eigenvector of the stationary point **4**. This gives a set of normal-mode kinetic energies at time t . This is repeated over a time interval t_{avg} that is longer than the vibrational period of the lowest frequency mode of **4**. For each mode, the kinetic energy is averaged over t_{avg} to get the mean kinetic energy of each mode. With the assumption that equipartition of kinetic and potential energy is valid over t_{avg} , the mean kinetic energy of each mode is multiplied by 2 to get the mode energy.

The Raff procedure implicitly assumes that the coordinates at each point are oriented to match the orientation of the **4** stationary point as much as possible. This is accomplished by rotating the instantaneous coordinates and momenta to the Eckart frame,^{59,60} which minimizes the root-mean-square deviation from the equilibrium geometry of **4** in mass-weighted Cartesian coordinates.⁶¹ We used the quaternion method for rotating to the Eckart frame.⁶²

RRKM Calculations. RRKM calculations were carried out using an available program⁶³ and employing the Beyer–Swinehart direct count algorithm.⁶⁴ The intermediate **4** was used as the starting point for the rate calculations and the energy employed was the zero-point-corrected energy difference between 3^\ddagger and **4**.

■ ASSOCIATED CONTENT

● Supporting Information

Cartesian coordinates; absolute energies, enthalpies, free energies, entropies, and lowest frequencies of calculated structures; single-point energetics by various methods; summary of calculated QCTs; and Master Equation calculations. This material is available free of charge via the Internet at <http://pubs.acs.org>.

■ AUTHOR INFORMATION

Corresponding Author

*houk@chem.ucla.edu

Notes

The authors declare no competing financial interest.

■ ACKNOWLEDGMENTS

This work was supported by the National Science Foundation (CHE 1361104 and CHE 1059084 to K.N.H.; CHE-1213976 to C.D). Calculations were performed on the Hoffman2 cluster at UCLA and the Extreme Science and Engineering Discovery Environment (XSEDE), which is supported by the National Science Foundation (OCI-1053575).

■ REFERENCES

- (1) Carboni, R. A.; Lindsey, R. V. *J. Am. Chem. Soc.* **1959**, *81*, 4342–4346.
- (2) Sauer, J.; Heldmann, D. K.; Hetzenegger, J.; Krauthan, J.; Sichert, H.; Schuster, J. *Eur. J. Org. Chem.* **1998**, 1998, 2885–2896.
- (3) Thalhammer, F.; Wallfaher, U.; Sauer, J. *Tetrahedron Lett.* **1990**, *31*, 6851–6854.
- (4) Meier, A.; Sauer, J. *Tetrahedron Lett.* **1990**, *31*, 6855–6858.
- (5) Boger, D. L.; Panek, J. S.; Duff, S. R. *J. Am. Chem. Soc.* **1985**, *107*, 5745–5754.
- (6) Sakya, S. M.; Groskopf, K. K.; Boger, D. L. *Tetrahedron Lett.* **1997**, *38*, 3805–3808.
- (7) Boger, D. L.; Boyce, C. W.; Labroli, M. A.; Sehon, C. A.; Jin, Q. *J. Am. Chem. Soc.* **1999**, *121*, 54–62.
- (8) Benson, S. C.; Palabrica, C. A.; Snyder, J. K. *J. Org. Chem.* **1987**, *52*, 4610–4614.
- (9) Fu, L.; Gribble, G. W. *Tetrahedron Lett.* **2010**, *51*, 537–539.
- (10) Blackman, M. L.; Royzen, M.; Fox, J. M. *J. Am. Chem. Soc.* **2008**, *130*, 13518–13519.
- (11) Devaraj, N. K.; Weissleder, R.; Hilderbrand, S. A. *Bioconjugate Chem.* **2008**, *19*, 2297–2299.
- (12) Patterson, D. M.; Nazarova, L. A.; Xie, B.; Kamber, D. N.; Prescher, J. A. *J. Am. Chem. Soc.* **2012**, *134*, 18638–18643.
- (13) Yang, J.; Šečková, J.; Cole, C. M.; Devaraj, N. K. *Angew. Chem., Int. Ed.* **2012**, *51*, 7476–7479.
- (14) Thomas, J. D.; Cui, H.; North, P. J.; Hofer, T.; Rader, C.; Burke, T. R. *Bioconjugate Chem.* **2012**, *23*, 2007–2013.
- (15) Devaraj, N. K. *Synlett* **2012**, 23, 2147–2152.
- (16) Liang, Y.; Mackey, J. L.; Lopez, S. A.; Liu, F.; Houk, K. N. *J. Am. Chem. Soc.* **2012**, *134*, 17904–17907.
- (17) Kamber, D. N.; Nazarova, L. A.; Liang, Y.; Lopez, S. A.; Patterson, D. M.; Shih, H.-W.; Houk, K. N.; Prescher, J. A. *J. Am. Chem. Soc.* **2013**, *135*, 13680–13683.
- (18) Liu, F.; Paton, R. S.; Kim, S.; Liang, Y.; Houk, K. N. *J. Am. Chem. Soc.* **2013**, *135*, 15642–15649.
- (19) Sadasivam, D. V.; Prasad, E.; Flowers, R. A.; Birney, D. M. *J. Phys. Chem. A* **2006**, *110*, 1288–1294.
- (20) (a) Lyons, B. A.; Pfeifer, J.; Peterson, T. H.; Carpenter, B. K. *J. Am. Chem. Soc.* **1993**, *115*, 2427–2470. (b) Reyes, M. B.; Carpenter, B. K. *J. Am. Chem. Soc.* **2000**, *122*, 10163–10176. (c) Sorescu, D. C.; Thompson, D. L.; Raff, L. M. *J. Chem. Phys.* **1995**, *102*, 7910–7924.
- (21) Kleier, D. A.; Binsch, G.; Steigel, A.; Sauer, J. *J. Am. Chem. Soc.* **1970**, *92*, 3787–3789.
- (22) Chai, J.-D.; Head-Gordon, M. *Phys. Chem. Chem. Phys.* **2008**, *10*, 6615–6620.
- (23) Neese, F.; Schwabe, T.; Kossmann, S.; Schirmer, B.; Grimme, S. *J. Chem. Theory Comput.* **2009**, *5*, 3060–3073.
- (24) Scalmani, G.; Frisch, M. J. *J. Chem. Phys.* **2010**, *132*, No. 114110.
- (25) de Meijere, A. *Angew. Chem., Int. Ed. Engl.* **1979**, *18*, 809–886.
- (26) Peslherbe, G. H.; Wang, H. B.; Hase, W. L. *Monte Carlo sampling for classical trajectory simulations. Monte Carlo Methods in Chemical Physics*; John Wiley & Sons Inc.: New York, 1999; Vol. 105, pp 171–201.
- (27) Hase, W. L.; Duchovic, R. J.; Hu, X.; Komornicki, A.; Lim, K. F.; Lu, D.-h.; Peslherbe, G. H.; Swamy, K. N.; Linde, S. R. V.; Varandas, A.; Wang, H.; Wolf, R. J., Venus96: A general chemical dynamics

computer program. *Quantum Chemistry Program Exchange*; Indiana University: Bloomington, IN, 1996; Program No. QCPE 1671.

(28) Frisch, M. J.; Trucks, G. W.; Schlegel, H. B.; Scuseria, G. E.; Robb, M. A.; Cheeseman, J. R.; Scalmani, G.; Barone, V.; Mennucci, B.; Petersson, G. A.; Nakatsuji, H.; Caricato, M.; Li, X.; Hratchian, H. P.; Izmaylov, A. F.; Bloino, J.; Zheng, G.; Sonnenberg, J. L.; Hada, M.; Ehara, M.; Toyota, K.; Fukuda, R.; Hasegawa, J.; Ishida, M.; Nakajima, T.; Honda, Y.; Kitao, O.; Nakai, H.; Vreven, T.; Montgomery, J. A., Jr.; Peralta, J. E.; Ogliaro, F.; Bearpark, M.; Heyd, J. J.; Brothers, E.; Kudin, K. N.; Staroverov, V. N.; Kobayashi, R.; Normand, J.; Raghavachari, K.; Rendell, A.; Burant, J. C.; Iyengar, S. S.; Tomasi, J.; Cossi, M.; Rega, N.; Millam, J. M.; Klene, M.; Knox, J. E.; Cross, J. B.; Bakken, V.; Adamo, C.; Jaramillo, J.; Gomperts, R.; Stratmann, R. E.; Yazyev, O.; Austin, A. J.; Cammi, R.; Pomelli, C.; Ochterski, J. W.; Martin, R. L.; Morokuma, K.; Zakrzewski, V. G.; Voth, G. A.; Salvador, P.; Dannenberg, J. J.; Dapprich, S.; Daniels, A. D.; Ö. Farkas, Foresman, J. B.; Ortiz, J. V.; Cioslowski, J.; Fox, D. J. *Gaussian 09*, Revision A; Gaussian Inc., Wallingford, CT, 2009.

(29) Millam, J. M.; Bakken, V.; Chen, W.; Hase, W. L.; Schlegel, H. B. *J. Chem. Phys.* **1999**, *111*, 3800–3805.

(30) Jiménez-Osés, G.; Liu, P.; Matute, R. A.; Houk, K. N. *Angew. Chem., Int. Ed.* **2014**, *53*, 8664–8667.

(31) Black, K.; Liu, P.; Xu, L.; Doubleday, C.; Houk, K. N. *Proc. Natl. Acad. Sci. U.S.A.* **2012**, *109*, 12860–12865.

(32) (a) Xu, L.; Doubleday, C. E.; Houk, K. N. *J. Am. Chem. Soc.* **2011**, *133*, 17848–17854. (b) Xu, L.; Doubleday, C. E.; Houk, K. N. *J. Am. Chem. Soc.* **2010**, *132*, 3029–3037. (c) Xu, L.; Doubleday, C. E.; Houk, K. N. *Angew. Chem., Int. Ed.* **2009**, *48*, 2746–2748.

(33) Zhu, L.; Hase, W. L., A General RRKM Program. *Quantum Chemistry Program Exchange*; Indiana University: Bloomington, IN, 1994; Program No. QCPE 1644.

(34) Beyer, T.; Swinehart, D. F. *Commun. Assoc. Comput. Machin.* **1973**, *16*, 379–379.

(35) Nummela, J. A.; Carpenter, B. K. *J. Am. Chem. Soc.* **2002**, *124*, 8512–8513.

(36) Litovitz, A. E.; Keresztes, L.; Carpenter, B. K. *J. Am. Chem. Soc.* **2008**, *130*, 12085–12094.

(37) (a) Goldman, L. M.; Glowacki, D. R.; Carpenter, B. K. *J. Am. Chem. Soc.* **2011**, *133*, 5312–5318. (b) Carpenter, B. K. *Chem. Rev.* **2013**, *113*, 7265–7286.

(38) Sun, L.; Hase, W. L. *J. Chem. Phys.* **2004**, *121*, 8831–8845.

(39) Sun, L.; Park, K.; Song, K.; Setser, D. W.; Hase, W. L. *J. Chem. Phys.* **2006**, *124*, No. 064313.

(40) Vayner, G.; Addepalli, S. V.; Song, K.; Hase, W. L. *J. Chem. Phys.* **2006**, *125*, No. 014317.

(41) (a) Doubleday, C.; Bolton, K.; Peslherbe, G. H.; Hase, W. H. *J. Am. Chem. Soc.* **1996**, *118*, 9922–9931. (b) Park, K.; Engelkemier, J.; Persico, M.; Manikandan, P.; Hase, W. L. *J. Phys. Chem. A* **2011**, *115*, 6603–6609.

(42) Zheng, J.; Papajak, E.; Truhlar, D. G. *J. Am. Chem. Soc.* **2009**, *131*, 15754–15760.

(43) Oyola, Y.; Singleton, D. A. *J. Am. Chem. Soc.* **2009**, *131*, 3130–3131.

(44) Glowacki, D. R.; Liang, C. H.; Marsden, S. P.; Harvey, J. N.; Pilling, M. J. *J. Am. Chem. Soc.* **2010**, *132*, 13621–13623.

(45) Glowacki, D. R.; Liang, C.-H.; Morley, C.; Pilling, M. J.; Robertson, S. H. *J. Phys. Chem. A* **2012**, *116*, 9545–9560.

(46) Zewail, A. H. *Angew. Chem., Int. Ed.* **2000**, *39*, 2586–2631.

(47) Cho, Y.; Van de Linde, S. R.; Zhu, L.; Hase, W. L. *J. Chem. Phys.* **1992**, *96*, 8275–8287.

(48) Sun, L.; Hase, W. L.; Song, K. *J. Am. Chem. Soc.* **2001**, *123*, 5753–5756.

(49) Cheon, S.; Song, K.; Hase, W. L. *J. Mol. Struct.: Theochem* **2006**, *771*, 27–31.

(50) Dunning, G. T.; Glowacki, D. R.; Preston, T. J.; Greaves, S. J.; Greetham, G. M.; Clark, I. P.; Towrie, M.; Harvey, J. N.; Orr-Ewing, A. *J. Science* **2015**, *347*, 530–533.

(51) Carpenter, B. K.; Harvey, J. N.; Glowacki, D. R. *Phys. Chem. Chem. Phys.* **2015**, DOI: 10.1039/C4CP05078A.

(52) Zhao, Y.; Truhlar, D. *Theor. Chem. Acc.* **2008**, *120*, 215–241.

(53) Lan, Y.; Zou, L.; Cao, Y.; Houk, K. N. *J. Phys. Chem. A* **2011**, *115*, 13906–13920.

(54) Paton, R. S.; Mackey, J. L.; Kim, W. H.; Lee, J. H.; Danishefsky, S. J.; Houk, K. N. *J. Am. Chem. Soc.* **2010**, *132*, 9335–9340.

(55) Ribeiro, R. F.; Marenich, A. V.; Cramer, C. J.; Truhlar, D. G. *J. Phys. Chem. B* **2011**, *115*, 14556–14562.

(56) Lee, C.; Yang, W.; Parr, R. G. *Phys. Rev. B* **1988**, *37*, 785–789.

(57) Pieniazek, S. N.; Clemente, F. R.; Houk, K. N. *Angew. Chem., Int. Ed.* **2008**, *47*, 7746–7749.

(58) Raff, L. *J. Chem. Phys.* **1988**, *89*, 5680–5691.

(59) Eckart, C. *Phys. Rev.* **1935**, *47*, 552.

(60) (a) Dymarsky, A. Y.; Kudin, K. K. *J. Chem. Phys.* **2005**, *122*, No. 124103. (b) Kudin, K. K.; Dymarsky, A. Y. *J. Chem. Phys.* **2005**, *122*, No. 224105.

(61) Jorgensen, F. *Int. J. Quantum Chem.* **1978**, *14*, 55.

(62) <http://www.ccl.net/cca/software/SOURCES/FORTRAN/fitest/fitest.shtml>

(63) Zhu, L.; Hase, W. L., A General RRKM Program. *Quantum Chemistry Program Exchange*; Indiana University: Bloomington, IN, 1994; Program No. QCPE 1644.

(64) Beyer, T.; Swinehart, D. F. *Commun. Assoc. Comput. Machin.* **1973**, *16*, 379–379.